

PAPER

## Formation of smoother grain boundaries in 2D materials using high deposition rates during the last stages of growth

To cite this article: Fabio D A Aarão Reis *et al* 2022 *2D Mater.* **9** 045025

View the [article online](#) for updates and enhancements.

### You may also like

- [Effect of grain boundary direction on blistering in deuterium-exposed tungsten materials: Parallel grain boundary versus perpendicular grain boundary](#)

Mi Liu, Long Cheng, Yue Yuan *et al.*

- [Electronic transport across extended grain boundaries in graphene](#)

Arnab K Majee and Zlatan Aksamija

- [Ab initio study of symmetrical tilt grain boundaries in bcc Fe: structural units, magnetic moments, interfacial bonding, local energy and local stress](#)

Somesh Kr Bhattacharya, Shingo Tanaka, Yoshinori Shiihara *et al.*

## 2D Materials



### PAPER

RECEIVED  
13 April 2022

REVISED  
23 August 2022

ACCEPTED FOR PUBLICATION  
31 August 2022

PUBLISHED  
16 September 2022

# Formation of smoother grain boundaries in 2D materials using high deposition rates during the last stages of growth

Fabio D A Aarão Reis<sup>1,\*</sup> , Bastien Marguet<sup>2</sup> and Olivier Pierre-Louis<sup>2</sup> 

<sup>1</sup> Instituto de Física, Universidade Federal Fluminense, Avenida Litorânea s/n, 24210-340 Niterói, RJ, Brazil

<sup>2</sup> Institut Lumière Matière, UMR5306 Université Lyon 1—CNRS, Villeurbanne 69622, France

\* Author to whom any correspondence should be addressed.

E-mail: [fdaar@protonmail.com](mailto:fdaar@protonmail.com)

**Keywords:** grain boundary, roughness, coverage, grain growth, kinetic Monte Carlo, deposition rate

Supplementary material for this article is available [online](#)

### Abstract

Grain boundary (GB) roughness can affect electronic and mechanical properties of two-dimensional materials. This roughness depends crucially on the growth process by which the two-dimensional material is formed. To investigate the key mechanisms that govern the GB roughening, we have performed kinetic Monte Carlo simulations of a simple model that includes particle attachment, detachment, and diffusion. We have studied the closure of the gap between two flakes during growth, and the subsequent formation of the GB for a broad range of model parameters. The well-known near-equilibrium (attachment-limited) and unstable (diffusion-limited) growth regimes are identified, but we also observe a third regime when the precursor flux is sufficiently high to saturate the gap between the edges with diffusing species. This high deposition rate regime forms GBs with spatially uncorrelated roughness, which quickly relax to smoother configurations. Extrapolating the numerical results (with support from a theoretical approach) to edge lengths and gap widths of some micrometres, we confirm the advantage of this regime to produce GBs with minimal roughness faster than near-equilibrium conditions. This suggests an unexpected route towards efficient growth of two-dimensional materials with smooth GBs.

### 1. Introduction

The variety of applications of two-dimensional (2D) materials such as graphene and transition metal dichalcogenides (TMDs) has motivated several studies of their growth kinetics in the last two decades [1–5]. The growth of large grains is frequently desired to reduce the effects of grain boundaries (GBs) on the electronic and mechanical properties. However, in some materials, a large GB density may be a minor problem; this is the case for the integration of ultrathin MoS<sub>2</sub> films with Si substrates in some devices that require low temperature deposition [6]. Moreover, large GB densities may be beneficial for some applications of 2D materials, such as WS<sub>2</sub> in sensors of Hg [7] and MoS<sub>2</sub> in the production of memtransistors [8]. GBs of WS<sub>2</sub> may also be useful as high conductivity channels [9].

Beyond the GB density, the GB roughness may also affect the properties of 2D materials in nontrivial

ways. Sinusoidal graphene GBs are advantageous over atomically flat GBs because they increase the mechanical strength and improve electronic properties [10]. The fractures of ReS<sub>2</sub> monolayers more easily occur at GBs parallel to Re chains [11], so that disordered GBs may improve their properties. In the case of graphene, there is also evidence that the grain size at the micrometer scale does not have relevant effects on the electric conductivity [12] and that the mechanical strength is not reduced in the presence of GBs [13].

The GB morphology is strongly related to the growth conditions and several models were already proposed to explain this relation [1, 3]. For sufficiently slow graphene growth, the so-called attachment limited (or near-equilibrium) conditions are observed, which usually lead to formation of smooth GBs. Models of step flow describe the edge propagation [14] and the GB structure can be determined by the misorientation angle [15] in these conditions. Similar models and other multi-scale approaches are

used to describe the growth of 2D TMDs [16–18]. However, fast growth is frequently important for applications. In this case, the so-called diffusion limited regime is frequently observed, in which GBs significantly deviate from a straight profile [19]. Experiments, phase field models, and kinetic Monte Carlo (kMC) simulations show formation of grains with fractal or dendritic morphologies that reproduce experimental observations [3, 17, 20–25].

The recurrent observation of similar relations between the GB morphology and the growth conditions in a wide variety of materials is a motivation for the study of models that only contain the essential physico-chemical mechanisms that are needed to explain those relations. This reasoning has already been successful in the description of the morphology of homoepitaxial metal and semiconductor films by means of generic models including adatom diffusion and attachment/detachment from islands and terraces [26–31].

In this work, we introduce a model for the propagation of two grain edges and for the relaxation of the GB formed after the collision of those edges. The aim of the model is to identify the generic consequences of elementary microscopic processes such as adatom surface diffusion, attachment, and detachment from edges and GBs of a variety of 2d materials, in contrast with approaches that focus on particular applications [15, 16, 25, 32, 33]. This modelling approach allows one to investigate the effects of the variations of the rates of those processes over several orders of magnitude using kMC simulations.

The simulations reproduce the main features of the regimes limited by attachment and diffusion described above, respectively for low and high fluxes. However, if the precursor flux is sufficiently high for the concentration of diffusing species to reach full saturation on the substrate surface, a nontrivial regime is observed: after an uncorrelated growth of the edges, the relaxation forms relatively smoother GBs at relatively shorter times compared to the other regimes. From the simulation results at nanoscale and the support of a theoretical approach, extrapolations to micrometre sized edges separated by micrometre sized gaps are performed. They show the possible advantages of increasing the deposition rate beyond the diffusion limited regime for reducing the GB roughness.

## 2. Model and methods

### 2.1. Model for deposition, diffusion, and aggregation

The solid structure is modelled by a square lattice, which differs from the geometry of most 2D materials, but is amenable to computational and analytical calculations. Each lattice site may be empty or occupied by a particle, which may represent a graphene atom or a TMD molecule. The lattice constant is

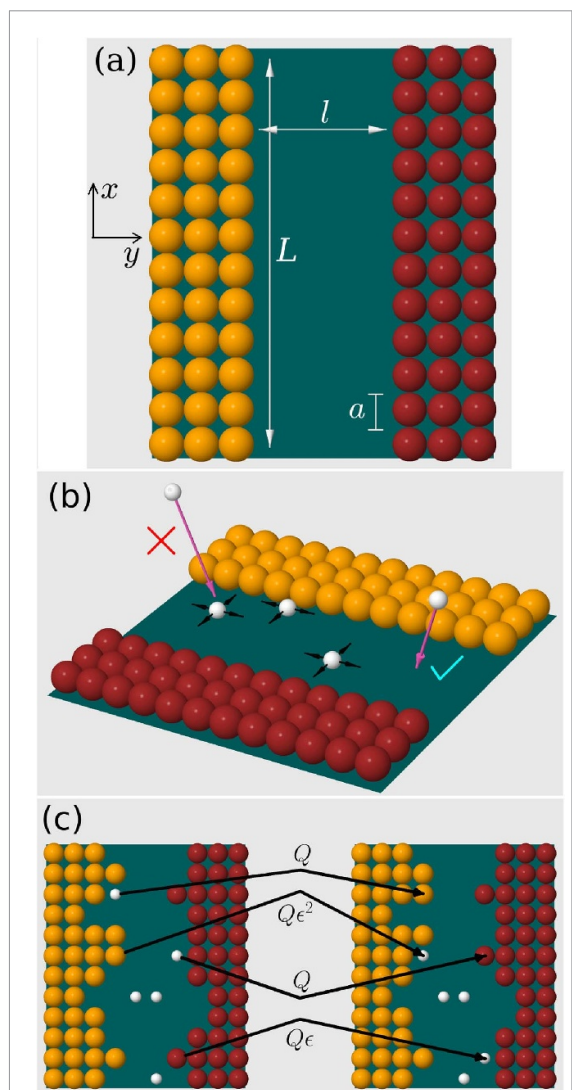


**Figure 1.** (a) Initial configuration of the grains A (yellow) and B (red). (b) Two particles inside at the gap (magenta arrows), the right one is accepted and the left one is rejected (excluded volume). Possible hops of particles already deposited in the gap are also indicated (black arrows). (c) Rates of the processes that bring the configuration at the left to the configuration at the right.

denoted as  $a$ . The atoms of the substrate below this square lattice are assumed to be immobile.

Two solid grains have initially straight interfaces (edges) of length  $L$  along the  $x$  direction and are separated by a gap of width  $l$ , as illustrated in figure 1(a). Periodic boundaries are considered in the  $x$  direction. Each aggregated particle is labelled with an index, A or B, which depends on the grain. Once new particles are incorporated in a grain, they receive the corresponding label. These indices are kept even after the complete filling of the gap and the attachment of all deposited particles, so that the two grains do not coalesce into a single grain.

The external particle flux  $F$  is the number of incident particles per site per unit time. If the incident particle reaches an empty site above the substrate, it becomes a mobile particle at that position; however, if it reaches an occupied site, the deposition attempt

is rejected. This process is illustrated in figure 1(b). A mobile particle represents an atom or a molecule that transports the constituents of the grains but which is not bonded (attached) to a grain.

The mobile particles can diffuse on the substrate, with a hopping rate to nearest neighbour (NN) sites per unit time equal to  $D$ . A hop attempt is executed only if the target site is empty, otherwise the mobile particle remains in the same position. The process is also illustrated in figure 1(b). The corresponding tracer diffusion coefficient is  $Da^2/4$ . The assumption that the excluded volume is the only type of interaction between mobile particles implies that other islands or grains are not formed in the gap.

The grains evolve via the attachment of mobile particles and detachment of aggregated particles. To facilitate the connection with kinetic roughening theory and other analytical approaches, these processes in each grain are restricted to the topmost point in each lateral coordinate  $x$  (this is called the Solid-On-Solid constraint in the kMC and kinetic roughening literature [34, 35]). When a mobile particle is at the site immediately above the topmost grain particle, its attachment to the grain occurs with rate  $Q$ . Simultaneously, a topmost particle can detach from a grain with rate  $Q\epsilon^n$ , where  $n$  is the number of NNs of that grain and  $\epsilon < 1$  is termed the detachment probability per NN. These processes are illustrated in figure 1(c). With these rules, the attachment rate does not depend on the local configuration of the grain edge. However, the detachment is facilitated at edge tips ( $n = 1$ ) and is more difficult at straight regions ( $n = 3$ ).

After the edge collision, the boundary between the grains A and B is formed. The above rules for attachment and detachment are maintained and the interactions between particles of different grains are restricted to excluded volume interactions. This means that the formation of bonds between NN particles of different grains is neglected. This may be a reasonable approximation if the actual inter-grain bonds of a material are sufficiently weak in comparison with the intra-grain bonds. In this approximation, the characteristic time scales of the grain edge dynamics are not much different before and after the collision.

The diffusion and detachment of particles are expected to be temperature activated processes, so that the rates  $D$  and  $\epsilon$  increase as the temperature increases. In many systems, the attachment is also activated, so  $Q$  also increases with the temperature. These parameters may then be written in Arrhenius forms (see section S.I of the supplementary material). It defines a true thermodynamic equilibrium in the model without deposition, which is enforced by detailed balance. However, since our aim is to address possible properties of several 2D materials, we do not choose a set of activation energies for the simulations, but study a large variety of possible relations between those rates and the flux  $F$ .

## 2.2. Scope of the model

Large scale and long-time properties of growth models are independent of the particular choice of the lattice geometry [29, 34]. For instance, interface roughness is one of the properties which are known to exhibit such universal behaviour [34, 35]. Hence, the regimes that emerge from our model based on a simple square lattice should generalize to other 2D lattices. The present model also benefits from a large number of previous theoretical investigations [28] and we will build up on this body of knowledge to derive some results analytically. These derivations could guide future investigations of models for specific materials.

The growth of different 2D materials involves different, possibly complex mechanisms of transport and reaction on surfaces. The model rules for the particle flux, the formation of mobile particles on the exposed substrate, their diffusion, and their attachment to the grains are minimal ingredients that are expected to catch the essential behaviours emerging from those complex processes. This assumption is based on the concept of separation of scales: when a process is much slower than the other ones, the concentrations of some species can be eliminated and a reduced set of mechanisms dictate the global dynamical behaviour of the system [36].

For example, in the case of graphene growth from methane gas, a sequence of reactions involving several molecules occurs at the substrate surface [37] and at the graphene edge [38]. The rates of diffusion and reaction depend strongly on physical parameters such as temperature, surface oxygen concentration [19, 25], and partial  $H_2$  pressure [39]. In this context, our model is directly applicable if the impinging species reacts quickly when it is adsorbed on the substrate, giving rise to growth units that diffuse up to the grain edges, where they may react. Those growth units are represented here by the mobile particles. The model is also applicable when the reactions that form the growth units occur in the vapor phase and the only surface reactions are those of bond formation at grain edges; this is the case of  $ReS_2$  growth if the molecules are formed from mixed  $Re$  and  $S$  gases [40]. Moreover, the model also applies if adsorbed molecules quickly diffuse and are in equilibrium with the vapour phase while releasing growth units homogeneously on the substrate surface. We therefore see our one-species model as a simple paradigm that may emerge from the growth of several 2D materials such as graphene and TMDs.

The interactions between the deposited material and the substrate are restricted to its catalytic effect on the reactions of the precursors, which produce the mobile particles, and to the presence of an energy barrier for the diffusion of the mobile particles, which sets the value of the coefficient  $D$  (section S.I of the supplementary material). Substrate-grain interactions are assumed to be sufficiently strong to prevent

grain diffusion. Furthermore, we assume initially straight and parallel grain edges because the model aims at describing the late stages of edge propagation and the subsequent relaxation of the GBs, but does not aim at describing grain nucleation and growth.

Finally, the mechanisms of GB relaxation are simplified because our aim is to determine large scale and long-time features of GB reshaping in different conditions of edge collision (e.g. to compare evolutions after diffusion-limited and attachment-limited growth). The absence of grain coalescence is a reasonable assumption in the case of grains with different crystallographic orientations or with some mismatch. Note that imperfect match of 2D grains may also occur when they have the same orientation, as observed in  $WS_2$  growth on sapphire [18].

### 2.3. Simulations and quantities of interest

Simulations were performed in lattices with edge length  $L$  varying from  $128a$  to  $1024a$ ; most results are obtained for  $L = 512a$ . The initial gap width  $l$  varies between  $16a$  and  $128a$ . The model rates in the simulations are measured in terms of the flux rate  $F$ . The ratios  $F/D$  and  $F/Q$  vary from  $10^{-8}$  to  $10^4$ ; these limiting values respectively represent very low and very high fluxes for a given temperature. Most simulations are performed with  $\epsilon = 0.1$ , which implies that the detachment rates have a weak dependence on the coordination number  $n$ ; this is reasonable only at high temperatures for most materials ( $k_B T \approx 0.43$  times the activation energy per NN). Additional simulations were performed with  $0.01 \leq \epsilon \leq 0.07$  to analyse the effects of this parameter.

For most parameter sets, average quantities are calculated over 100 different configurations, but in some cases  $10^3$ – $2 \times 10^3$  configurations are considered. The kMC algorithm developed for these simulations is similar to that of previous works on sub-monolayer growth [41–43].

The main quantity calculated here is the roughness of the grain edges. Letting  $h(x, t)$  to denote the height of an edge at position  $x$  and time  $t$  measured relatively to its initial position, the roughness is defined as:

$$W \equiv \langle \overline{(h - \bar{h})^2} \rangle^{1/2}, \quad (1)$$

where the overbars denote a spatial average (over the values of  $x$  in a given sample) and the angular brackets denote a configurational average (over different samples). Due to the symmetry of the grains A and B, our configurational average also includes averaging over the two grains of each growing sample.

The gap coverage is defined as the fraction of the initial gap covered by deposited particles:

$$\theta = \frac{N_d}{(Ll/a^2)}, \quad (2)$$

where  $N_d$  is the total number of deposited particles, mobile or aggregated, and  $Ll$  is the initial gap area. When the deposition begins,  $t = 0$ , the gap coverage is  $\theta = 0$ , which shows that this quantity does not account for the fraction of the substrate covered by the initial grains (such a fraction is not defined in the present model). Since deposition of new particles can only occur in empty sites, the deposition stops when the gap coverage is  $\theta = 1$ . However, observe that particle attachment and detachment do not affect the value of  $\theta$ .

To characterize the transition from edge growth (when attachment dominates over detachment) to GB relaxation (when the grains evolve with balanced attachment and detachment), we define an average collision time  $t_c$ . For each position  $x$  and a given configuration of evolving grains, the local collision time  $t_c^{(local)}(x)$  is defined as the first time in which grains A and B occupy NN sites at position  $x$  (with any value of  $y$ ). Observe that the GB is not frozen after collision, so particles may detach from one of the grains, move to NN sites, or reattach to one of the two grains. The value of  $t_c$  is obtained by averaging  $t_c^{(local)}$  over all positions  $x$  and over different configurations of evolving grains; this averaging also gives the standard deviation of the collision times,  $\Delta t_c$ .

## 3. Results and discussion

### 3.1. Morphological evolution

Figures 2(a)–(c) show snapshots of the deposits grown with different values of the incident flux but with constant values of  $D$ ,  $Q$ , and  $\epsilon$ , which are set to  $Q/D = 10^{-1}$  and  $\epsilon = 0.1$ . This is expected to mimic constant temperature conditions with variable precursor fluxes. The growth times are shown in dimensionless units of  $Dt$ .

For the lowest flux ( $F/D = 10^{-6}$ ), figure 2(a) shows that the roughness of the growing edges is dominated by long wavelength fluctuations. The peaks and valleys evolve from typical sizes  $10a$ – $30a$  at  $Dt = 5 \times 10^5$  to sizes larger than  $30a$  at  $Dt = 2 \times 10^6$ , but no significant change in the edge roughness is visible. The particle density in the gap is very small until the grain collision; this is confirmed by the magnified view in figure 3(a) of the region highlighted in figure 2(a). Similar evolution is observed for larger diffusion coefficients of the particles in the gap, i.e. when  $Q/D$  and  $F/D$  decrease by the same factor, as shown in section S.II of the supplementary material. These features are representative of the attachment limited growth regime in this model.

As the gap is closed and a GB is formed, there is a drastic decrease of the boundary roughness. This decrease is also observed in models of collisions of uncorrelated interfaces that propagate with finite velocities and is independent of the detailed physics of their short range interactions [44]. After the collision, the GB evolves slowly by detachment of particles

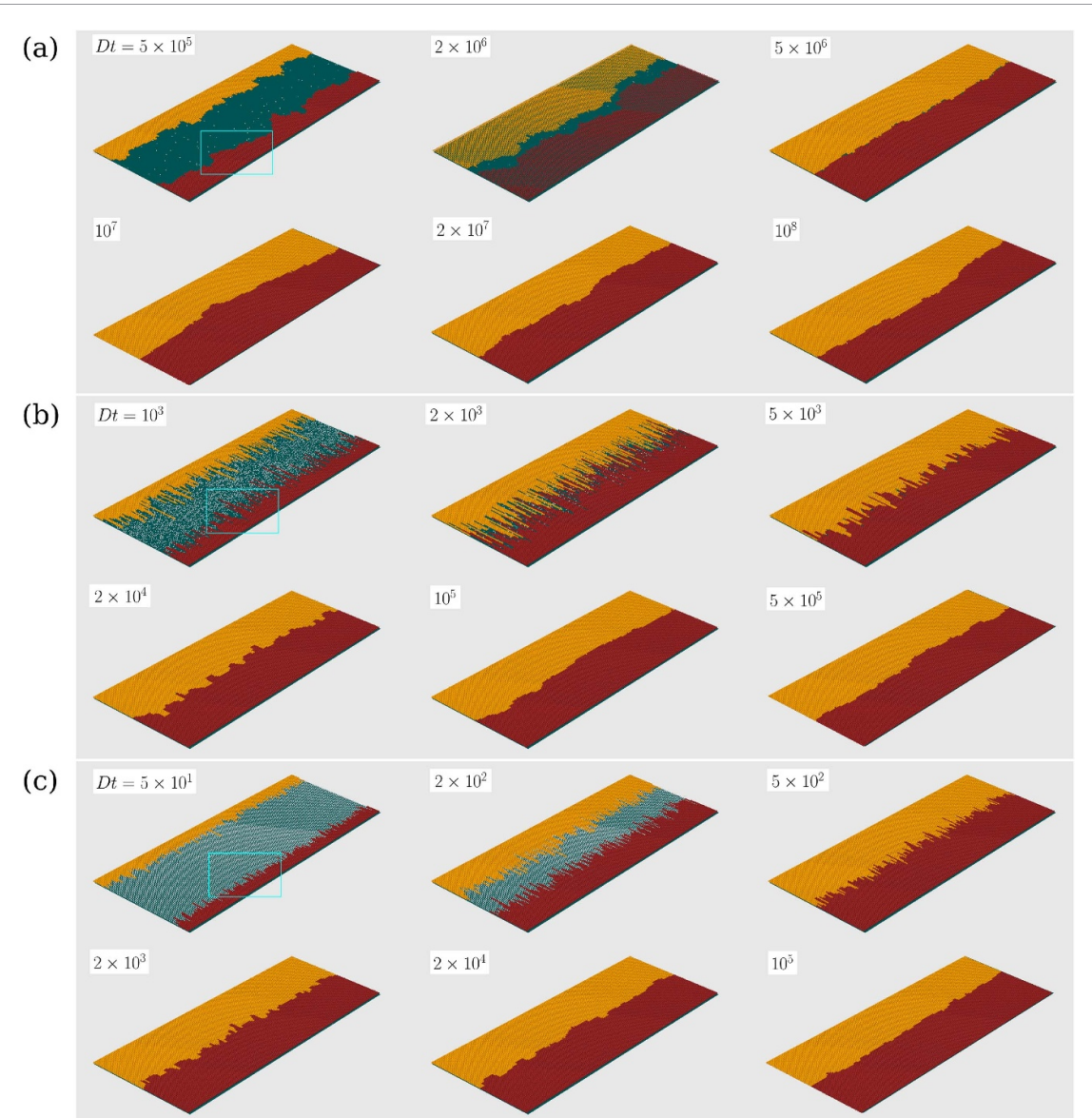


**Figure 2.** Snapshots of parts of the deposits grown with  $Q/D = 10^{-1}$ ,  $\epsilon = 0.1$ ,  $L = 1024a$ , and  $l = 128a$ : (a)  $F/D = 10^{-6}$ ; (b)  $F/D = 10^{-3}$ ; (c)  $F/D = 10$ . Light blue rectangles indicate the regions highlighted in figure 3.

from one edge followed by reattachment to the other, with apparently small changes in the roughness.

For the intermediate value of the flux ( $F/D = 10^{-3}$ ), but the same ratio  $Q/D$ , figure 2(b) shows spikes at the grain edges since early times. At  $Dt = 10^3$ , a high density of mobile particles is already present in the gap. Note that this time is much shorter than that of the first panel of figure 2(a). The magnified view in figure 3(b) shows that the mobile particle density is depleted only near the valleys of the grain edges. For this reason, the spikes grow faster than the valleys, as noticeable by comparing the snapshots at  $Dt = 10^3$  and  $2 \times 10^3$  in figure 2(b). This is characteristic of unstable growth in a diffusion-limited regime.

The spikes that result from the unstable growth are particular features of this model. They contrast with the fractal or dendritic shapes observed in experiments and in other models with unstable

growth [3, 17, 25]. This difference is a consequence of the condition that particle attachment occurs only at the topmost site at each  $x$ , which prevents the lateral attachment responsible for more complex morphologies.

When the gap is completely filled, the spikes remain, so the GB roughness is initially large. At  $Dt = 2 \times 10^4$ , figure 2(b) shows that the spikes are transformed to shorter and thicker structures. A smooth GB is achieved at  $Dt = 10^5$ , which is a much shorter time than that of the attachment-limited mode shown in figure 2(a).

Figure 2(c) shows results for much higher flux,  $F/D = 10$ , but with the same  $Q/D$ . Now the particle attachment is very slow compared to the incoming flux. At a short time,  $Dt = 5 \times 10^1$ , the gap is completely covered with mobile particles (see the magnified view in figure 3(c)) and so it remains until those particles attach to the two edges, which collide and

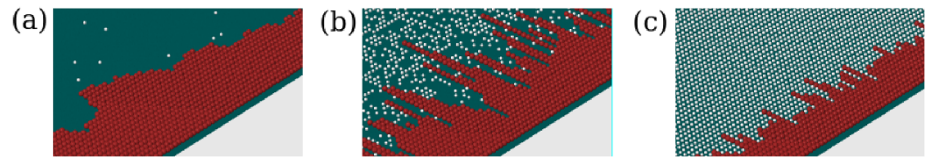


Figure 3. (a)–(c) Zooms of the regions indicated in figures 2(a)–(c), respectively.

form a GB. This contrasts with the diffusion-limited regime, in which the density was depleted near the edge valleys. In the present situation, the mobile particles are effectively static. Their attachment to the grain edges is equally probable at valleys and peaks because all edge sites are in contact with one of those particles. This gives rise to a spatially uncorrelated edge growth. Figure 2(c) also shows edges with spikes, but they are thinner and less protuberant than those of the diffusion-limited regime (figure 2(b)).

The GB is formed at  $Dt \sim 10^3$  with a non-negligible roughness. The relaxation of the GB leads to its smoothening. This process is comparably faster than that reported in figure 2(b), although the only relevant parameters,  $Q$  and  $\epsilon$ , are the same. Indeed, at  $Dt = 2 \times 10^4$ , the surface roughness in figure 2(c) is smaller than that observed in figure 2(b).

In section S.II of the supplementary material, we show that similar morphologies are obtained if the ratio  $Q/D$  decreases by a factor  $10^2$ , corresponding to a larger particle diffusivity. A full coverage of the gap is also attained at short times for a high value of the flux, which corresponds to the same ratio  $F/Q = 10^2$  of figure 2(c).

Thus, an apparently different growth regime is observed when the precursor flux is sufficiently high to fully cover the gap between the grains with mobile particles before a significant edge displacement. In this high deposition rate regime, where the substrate surface is rapidly saturated with material not aggregated to the grain edges, the GB may have an initially large roughness, but it attains smooth configurations in shorter times than those observed in diffusion-limited and attachment-limited regimes.

### 3.2. Roughness, coverage, and edge collision time

Figure 4(a) shows the time evolution of the roughness  $W$  of the grain edges for  $Q/D = 10^{-1}$ ,  $\epsilon = 0.1$ , initial gap width  $l = 64a$ , edge length  $L = 512a$ , and several values of  $F/D$ . For most of the flux values, figure 4(a) also indicates the typical ranges of edge collision times, which indicate the GB formation. Figure 4(b) shows the gap coverage  $\theta$  as a function of time for the same parameter sets.

In all cases,  $W$  increases during edge growth, as expected for any kinetic roughening process starting from a flat configuration [34, 35]. In most cases,  $W$  attains a maximal value near the average collision time (the only exception is the case with the lowest

flux, in which  $W$  seems to saturate after the initial increase). That result parallels the previous observation of a decrease of the roughness during the collision of interfaces propagating with constant velocities, independently of their short range interactions [44]; see also [45]. The smoothening or roughening processes that take place after the formation of the GB depend on the flux.

The lowest flux in figure 4(a),  $F/D = 10^{-6}$ , corresponds to the snapshots in figure 2(a). The plot shows that the initial near-equilibrium growth occurs with  $W \sim t^{1/4}$ . This is the roughening described by the Edwards–Wilkinson equation [46] at coarse grained scale, in which the surface tension and an uncorrelated noise are the main mechanisms. The relative fluctuation of the collision time is not large, as inferred by the width of the indicative bar in figure 4(a). After the GB formation, there are small changes in the roughness, which indicate that the GB attains a stationary regime.

The stationary regime can actually be mapped to a true thermodynamic equilibrium state, in which the roughness depends only on the detachment probability  $\epsilon$  and on the edge length  $L$ ; see details in section S.III of the supplementary material. For all values of the model rates ( $F$ ,  $D$ , and  $Q$ ) and of the initial gap width, the roughness is expected to converge to the same stationary value at sufficiently long times. Thus, depending on the maximal roughness attained before the grain collision,  $W$  may increase or decrease after formation of the GB. For instance, figure 4(a) shows that  $W$  increases towards the stationary value for  $F/D = 10^{-5}$  and  $F/D = 10^{-4}$ ; however, section S.IV of the supplementary material shows that  $W$  decreases towards the stationary value when the gap width is smaller.

For the intermediate flux,  $F/D = 10^{-3}$ , figure 4(a) shows that the initial increase of the roughness is faster than linear; it corresponds to the snapshots in figure 2(b). The explosive increase of height fluctuations confirms the unstable growth which is expected in a diffusion-limited regime. The range of collision times is broader in this case, as a consequence of the large dispersion in the local heights of the two edges. When the edges collide,  $W$  decreases and can reach much smaller values as the GB relaxes. After reaching a minimal value,  $W$  increases again (it is expected to converge to the stationary value at long times). In previous studies of sudden changes from

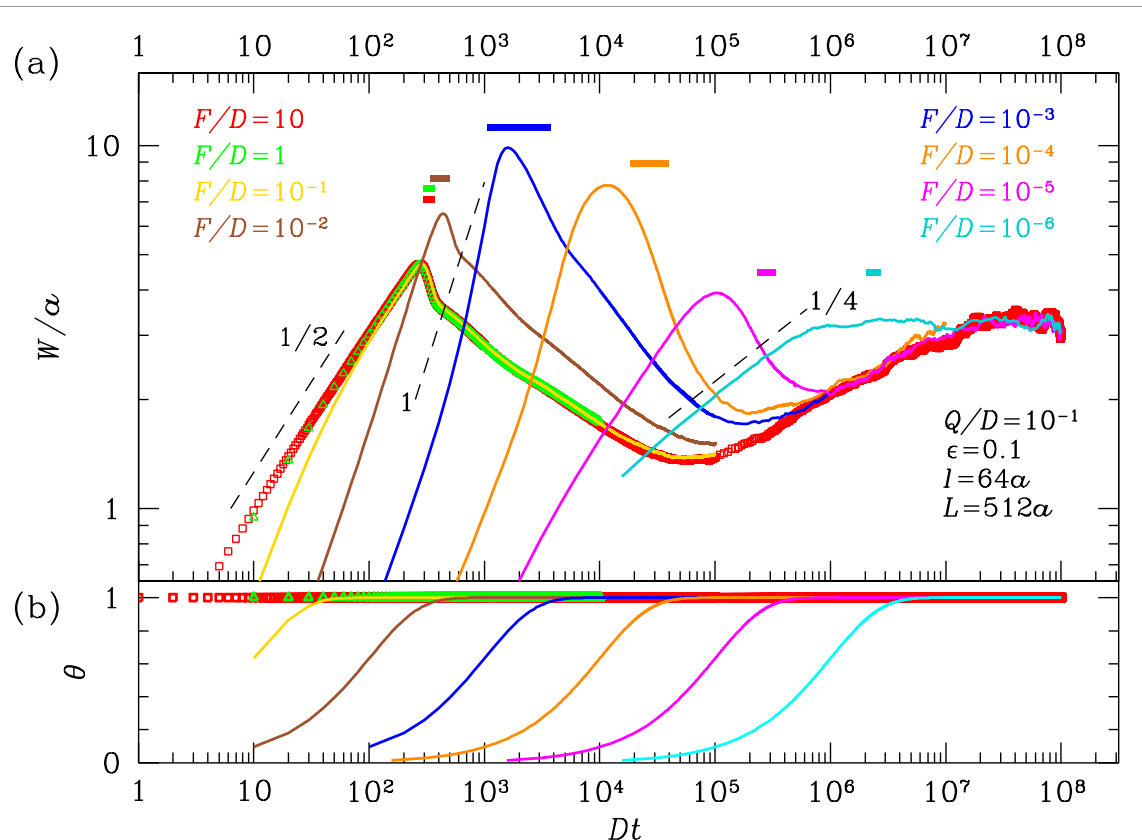


**Figure 4.** (a) Roughness evolution for constant  $Q/D = 10^{-1}$  and variable flux. Dashed lines with the indicated slopes are drawn for comparison with the slopes of the plots. Horizontal bars at  $W/a \lesssim 1$  indicate the edge collision times (average plus and minus one standard deviation). (b) Evolution of the gap coverage for the same parameter sets, with the same colour code of (a).

a first kinetics that produces faster roughening to a second kinetics that produces slower roughening, similar results were obtained, viz. rapid smoothening after the change and subsequent slow roughening [47, 48].

For the largest flux ( $F/D = 10$ ), the roughness in figure 4(a) approximately increases as  $W \sim t^{1/2}$ ; the corresponding snapshots are in figure 2(c). This is consistent with random uncorrelated deposition at both grain edges [34]. Figure 4(b) shows that full coverage of the gap ( $\theta \approx 1$ ) is attained long before the collision time, in contrast with the other regimes, in which  $\theta \approx 1$  only at times near the collision. This means that each site of the gap is occupied by a mobile (non-aggregated) particle at times so short that the edges had negligible displacements from their initial positions. Steric hindrance implies that the diffusion of those particles is suppressed. Growth of the 2D material then occurs via aggregation of those particles at the edges, which leads to uncorrelated roughening until some points of opposite edges collide.

In this high deposition rate regime, the maximal  $W$  is also attained near the collision time and the subsequent decrease is associated with the GB formation. The range of collision times is small compared to the other regimes. After the GB is formed, the roughness attains a minimum value which is smaller than the values obtained in the near-equilibrium and in the

diffusion-limited regimes. Moreover, this minimum value is attained in a shorter time compared to those regimes, as previously suggested by the snapshots of figures 2(a)–(c).

A common feature of the regimes limited by attachment and by diffusion is that the time of GB formation (the average collision time) is roughly proportional to the reciprocal of the flux rate:  $t_c \sim 3/F$ . The initial gap width and the mechanisms of particle diffusion, attachment, and detachment determine the edge morphology. However, in the high deposition rate regime, the time of GB formation depends on the rate  $Q$  but not on the flux  $F$ ; for instance, compare the data for  $F/D = 1$  and  $F/D = 10$  in figure 4(a). Indeed, as the gap is rapidly covered with mobile particles, the attachment controls the edge propagation; the effect of the diffusion rate is negligible because the mobile particle positions are effectively frozen. Thus, the collision time is inversely proportional to  $Q$  and proportional to the gap width  $l$ ; see details in section S.V of the supplementary material.

Between the three regimes described above, the roughness evolution shows crossover features. In figure 4(a),  $F/D = 10^{-5}$  and  $10^{-4}$  represent the crossover between the attachment-limited and the diffusion-limited regimes, whereas  $F/D = 10^{-2}$  and  $10^{-1}$  represent the crossover from the latter to the high deposition rate regime.

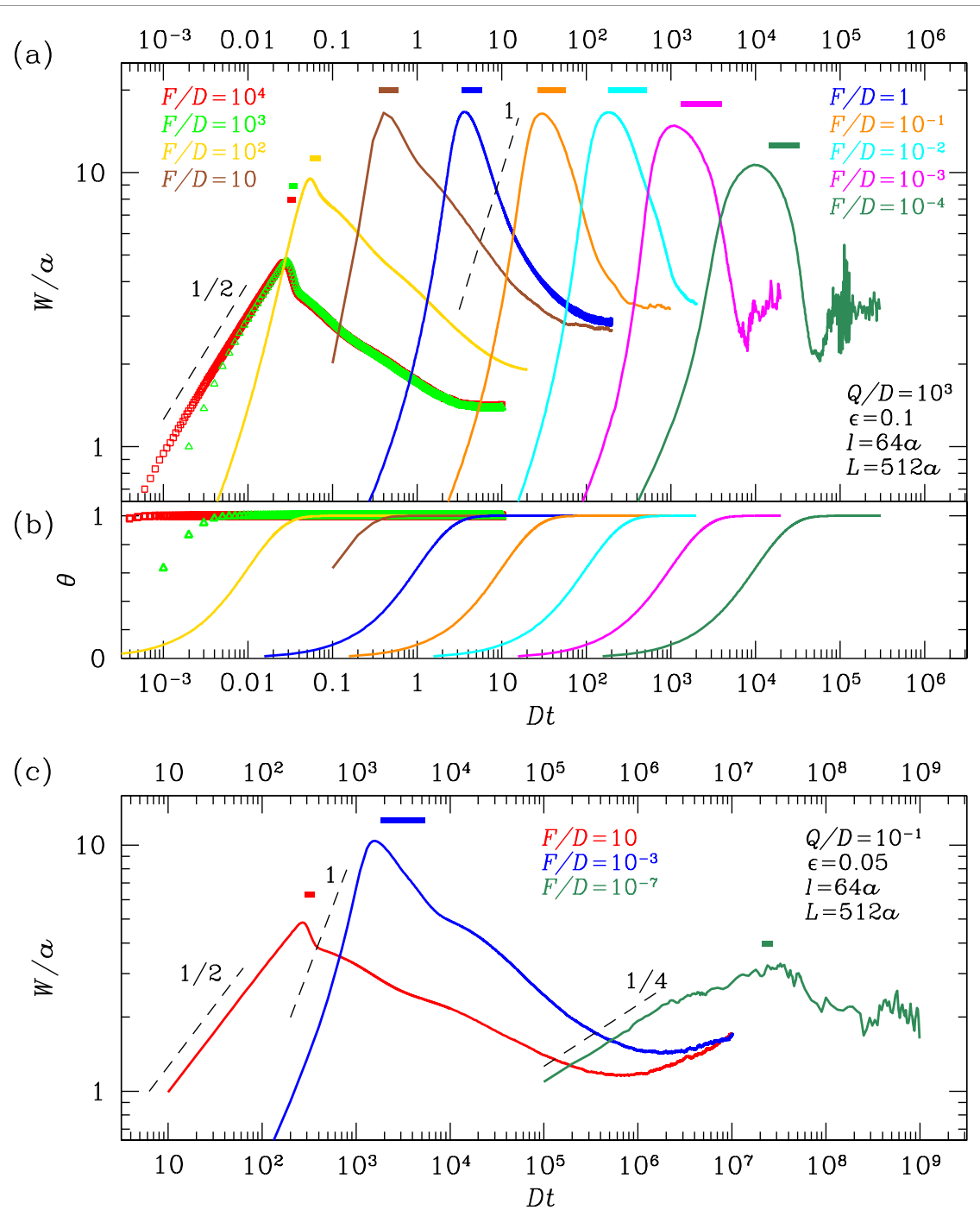


**Figure 5.** (a), (c) Roughness evolution for constant  $Q/D$  and variable flux. Dashed lines with the indicated slopes are drawn for comparison with the slopes of the plots. Horizontal bars at  $W/\alpha \lesssim 1$  indicate the edge collision times (average plus and minus one standard deviation). (b) Evolution of the gap coverage for the same parameters in (a), with the same colour code.

Qualitatively similar results are obtained for other ratios  $Q/D$ . Figure 5(a) shows the roughness evolution for several values of the flux  $F$  when  $Q/D = 10^3$ , which represents systems with very slow surface diffusion in comparison with the attachment and detachment rates; the other parameters remain the same as in figure 4(a) and the time scale of diffusion is also used for the data presentation. The main difference here is that the diffusion-limited (unstable) regime spans a broader range of  $F$ , since the slow diffusion favours the particle depletion near the edge valleys.

For this reason, no growth in the attachment-limited regime is observed in figure 5(a). However, for the highest flux  $F/D = 10^4$  (corresponding to  $F/Q = 10$ ), the features of the high deposition rate regime are also observed: long before the edges begin to move and to roughen ( $W/\alpha < 1$ ), the gap coverage reaches the value 1, as shown in figure 5(b); subsequently, the edges show the  $W \sim t^{1/2}$  scaling of uncorrelated growth; after the GB formation,  $W$  reaches a minimal value smaller than those attained in the other regimes, and this occurs at a shorter time.

Much larger diffusion coefficients (compared to the attachment rate) facilitate the particle redistribution in the gap and permit the observation of the attachment-limited regime, but suppress the unstable one (diffusion-limited). However, for the largest fluxes, the features of the high deposition rate regime are still observed because the diffusion is not effective in those cases. This is illustrated in section S.VI of the supplementary material for  $Q/D = 10^{-3}$ .

Changes in the gap width  $l$  affect the crossover between the diffusion-limited and the attachment-limited regimes, but also do not change the features of the high deposition rate regime. For smaller  $l$ , the unstable growth may not have sufficient time to develop, so the EW roughening of the edges is observed for slightly larger fluxes; see section S.IV of the supplementary material. Instead, for larger  $l$ , the unstable growth extends to smaller fluxes because the instability has longer time to develop before the edges collide.

Changes in the detachment probability  $\epsilon$  (which relates the detachment rates with the number of NNs) lead to some relevant changes in the roughness evolution, as shown in figure 5(c) for  $\epsilon = 0.05$  and the other parameters kept the same as in figure 4(a). First, a smaller  $\epsilon$  pushes the diffusion-limited regime to lower fluxes because the detachment kinetics of the edges is slower, but the attachment does not change. For this reason, a clear EW scaling of the roughness is observed only for  $F/D = 10^{-7}$  (in contrast with  $F/D = 10^{-6}$  for  $\epsilon = 0.1$ ; figure 4(a)). Second, for the intermediate and the largest fluxes, the smaller detachment rates lead to slower decays of the roughness after the GB formation. Despite these differences, the high deposition rate regime, which is obtained with the highest flux ( $F/D = 10$ ), still provides the smallest GB roughness during the relaxation.

For the largest flux in figure 5(c) ( $F/D = 10$ ), a nontrivial feature is the appearance of shoulders in the decay of the GB roughness. The decrease of the roughness upon the collision is a stochastic effect characteristic of interface collisions [44]. After that, the roughness decreases by the elimination of the thinnest spikes of the GB, which requires the detachment of particles with  $n = 1$  NN, whose rate is  $Q\epsilon$ . For small  $\epsilon$ , this rate is much smaller than that of the initial growth ( $Q$ ); the first shoulder is a consequence of the longer time scale associated to this process. Further relaxation of the GB depends on kink detachment (see section S.III of the supplementary material), whose rate is  $Q\epsilon^2$ . This is smaller than the rate of spike elimination by the factor  $\epsilon$ , which explains the second shoulder. These features become more pronounced for smaller  $\epsilon$ , as shown in section S.VII of the supplementary material; however, the highest deposition rate also provides the minimal roughness in a shorter time than the other growth regimes.

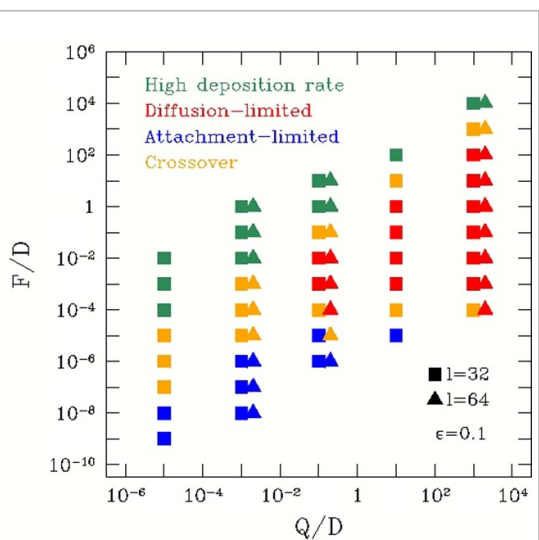


Figure 6. Grain growth regimes as function of the kinetic parameters for  $\epsilon = 0.1$  and two gap widths.

### 3.3. Phase diagram of grain edge growth

In our simulations, we identify three regimes of edge growth, i.e. before the edges begin to interact. The attachment-limited or near-equilibrium regime is characterized by slopes of the  $\log W \times \log(Dt)$  plots near the EW value  $1/4$ . The diffusion-limited or unstable regime is characterized by slopes larger than  $1$  at some time interval before the maximal  $W$ . Finally, the high deposition rate regime (or random growth) is characterized by slopes of the  $\log W \times \log(Dt)$  plots near  $1/2$ .

Figure 6 shows the phase diagram obtained with these criteria for  $\epsilon = 0.1$  and gap widths  $l = 32a$  and  $64a$ . For materials such as graphene or TMDs, the lattice constant is  $\sim 0.3$  nm, so those values correspond to widths  $\sim 10\text{--}20$  nm. Intermediate behaviours in figure 6 are considered as crossovers.

For very slow attachment-detachment kinetics in comparison with diffusion (very small  $Q/D$ ), the unstable growth is not observed because the mobile particles are uniformly distributed in the gap. The unstable growth is typically observed for  $F/Q \lesssim 0.1$  (to avoid the rapid uncorrelated growth),  $F/D \gtrsim 10^{-3}$  (to avoid very slow deposition, which favours near-equilibrium growth), and  $Q/D \gtrsim 1$  (fast interface kinetics compared to diffusion).

However, these conditions change as the gap width  $l$  or the detachment probability  $\epsilon$  change. For wider gaps, the instability has longer time to develop before the edge collision, so it can be observed for smaller values of  $F/D$ . As  $\epsilon$  decreases, particle detachment becomes slower, which also favours the instabilities; thus, the unstable regime can also be observed for smaller values of  $F/D$ .

The high deposition rate regime is more robust against changes in the physical or chemical parameters. It typically appears for  $F/Q \gtrsim 10$ , which is a condition in which the gap is almost completely

filled before the attachment of a single layer of particles at each edge. As explained before, the diffusion coefficient  $D$  is not important because the particles in the gap cannot move to the occupied NNs.

Experiments on 2D materials growth also reveal the existence of attachment-limited and diffusion-limited regimes [1, 3, 19–21, 24]. The rate limiting processes of each of those regimes have a parallel with those of our model [1]. The edge morphologies in experiments are different from those presented here, but the same qualitative trend of unstable roughening in attachment-limited conditions is observed. This confirms the reliability of the model for the qualitative prediction of large scale growth features. However, to our knowledge, the features of the regime of high deposition rates were not shown in previous models or in experiments on 2D materials growth.

### 3.4. The minimal GB roughness

In the simulations with high deposition rates ( $F/Q \gtrsim 10$ ), we measured the minimal value of the roughness obtained during the GB relaxation,  $W_{\min}$ , and the time in which this minimum was attained,  $t_{\min}$ .

$W_{\min}$  does not depend on the parameters  $F$ ,  $Q$ ,  $D$ , and  $L$ ; it is affected only by the detachment rate  $\epsilon$  and the gap width  $l$ . Figure 7(a) shows  $W_{\min}/a$  as a function of the scaling variable  $\epsilon l/a$ , i.e. the dimensionless product of the above parameters. Since the time of the minimal roughness rapidly increases as  $\epsilon$  decreases and the simulations become slower as  $l$  increases, we considered restricted ranges for those variables ( $0.05 \leq \epsilon \leq 0.1$  and  $16 \leq l \leq 64$ ) to obtain accurate estimates of  $W_{\min}$ . The linear fit in figure 7(a) gives the relation:

$$W_{\min} \approx 0.87 (\epsilon a^3 l)^{0.25}. \quad (3)$$

The dependence of  $W_{\min}$  on  $l$  can be explained by scaling arguments [47, 48]. From the initial flat edge condition to the edge collision, each of the grains is displaced by an average length  $l/2$ ; thus, the average number of particles attached to each column  $x$  of a grain is  $N = (l/2)/a$ . The uncorrelated growth in this regime leads to a maximal roughness of order [34]:

$$W_{\max} \sim a\sqrt{N} = \sqrt{\frac{al}{2}}, \quad (4)$$

the characteristic rate of this growth is  $Q$ . As the GB is formed, there is a sudden change from this uncorrelated growth to a correlated kinetics. If the characteristic rate of attachment and detachment of the final kinetics is the same as the initial one, the uncorrelated fluctuations are rapidly suppressed and the roughness rapidly reaches the same time evolution of the final kinetics starting from a flat interface (see e.g. figure 6

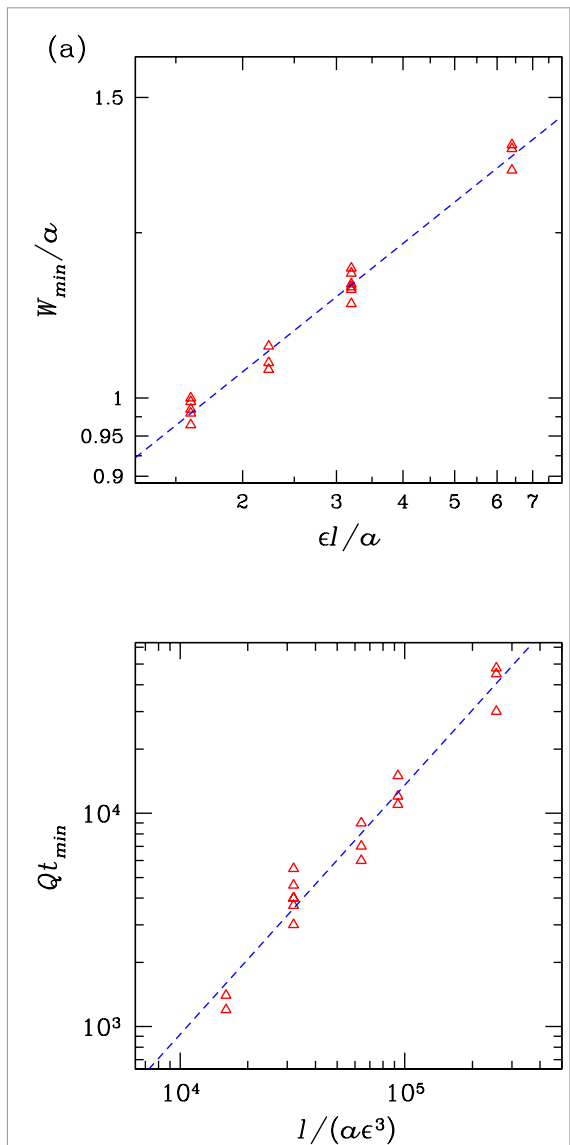


Figure 7. (a) Minimal roughness in the high deposition rate regime as a function of  $\epsilon l/a$ . The dashed line is a least squares fit with slope 0.25. (b) Scaled time of the minimal roughness as a function of  $l/(a\epsilon^3)$ . The dashed line is a least squares fit with slope 0.16.

of [47]); here, this would be the case of  $\epsilon \sim 1$ . The GB kinetics is EW (section S.III of the supplementary material), in which the growth from a flat interface leads to  $W \sim aN^{1/4}$ , where a prefactor of order 1 is excluded [34, 46]. The minimal roughness is then obtained by substituting the value of  $N$  at the collision time in this relation, which gives  $W_{\min} \sim l^{1/4}$ , consistently with equation (3).

However, to describe the GB relaxation with smaller  $\epsilon$ , a more powerful approach has to be used. We developed a Langevin model [49] which assumes that the GB evolution is controlled by kink site detachment from one grain (with characteristic rate  $Q\epsilon^2$ ) and attachment to the other grain. In section S.III of the supplementary material, this model is solved for an initial surface configuration with uncorrelated roughness  $W_{\max}$  and predicts:

$$W_{\min}^{(\text{Lang})} = \left[ \frac{1}{\pi(1-\epsilon)^2} \right]^{1/4} (a^3 l \epsilon)^{1/4}. \quad (5)$$

Since  $1 - \epsilon \approx 1$  is a reasonable approximation in our simulations, equation (5) leads to the same scaling in  $l$  and  $\epsilon$  of equation (3); the approximation gives a pre-factor 0.75, which is not distant from the numerical estimate 0.87 in equation (3).

The Langevin approach also predicts that the minimum roughness is attained at:

$$t_{\min}^{(\text{Lang})} = \frac{l}{2aQ} \left[ 1 + \frac{(1-\epsilon^2)}{8\epsilon^3} \right], \quad (6)$$

where the first term accounts for the uncorrelated growth of the edges of independent grains and the second one accounts for the coarsening of the GB. For  $\epsilon \ll 1$ , the first term is negligible in comparison with the second one, which gives  $t_{\min}^{(\text{Lang})} \approx l / (16aQ\epsilon^3)$ ; this is expected to be a reasonable approximation even for  $\epsilon = 0.1$ , which was considered in most simulations. Guided by this analytical result, figure 7(b) shows  $Qt_{\min}$  as a function of  $l/(a\epsilon^3)$ , which reasonably fits a straight line. The slope of that fit is 0.16, which is larger than, but of the same order of the theoretical slope 1/16.

### 3.5. Possible application to 2D materials growth

Here we discuss the application of the growth in the high deposition rate regime to produce 2D materials with small GB roughness. The notable properties of this regime do not seem to have been shown in previous works, in contrast to the attachment-limited and the diffusion-limited cases (which qualitatively parallel previous observations in experiments and models).

Equations (3) and (5) show that decreasing the growth temperature (so that  $\epsilon$  decreases) is advantageous for obtaining a smaller GB roughness. However, equation (6) shows that it is disadvantageous for increasing the time to attain this minimal roughness because  $Q$  and  $\epsilon$  decrease. Evidence on this disadvantage is provided by the comparison of figures 4(a) ( $\epsilon = 0.1$ ) and 4(c) ( $\epsilon = 0.05$ ) with figure S.6 of the supplementary material ( $\epsilon = 0.01$ ). The advantage involves a factor  $\epsilon^{1/4}$  and the disadvantage involves a factor  $1/(Q\epsilon^3)$ , so we generally expect that higher temperatures will be more favourable for obtaining smoother GBs. This implies that  $\epsilon$  and  $Q$  are large. However, the condition  $F/Q \gtrsim 10$  is also necessary to allow the initial uncorrelated growth of the separated grain edges (section 3.3).

For the application to a particular 2D material, it is necessary that isolated grains nucleate and grow to a configuration with smooth boundaries, which is the initial condition considered here; observe that the formation of this initial configuration is not addressed by our model. In such configuration, a

common situation is that the grains cover a fraction of the substrate  $\lesssim 0.1$ . The inspection of microscopy images with visible and isolated islands (grains) of 2D materials supports this estimate [1, 50–54]. Instead, with substrate coverages  $\sim 1$ , coalescence of several islands are observed. Thus, if the separated grains have typical boundary length  $L$ , the gap width  $l$  is expected to be of a similar order of magnitude; for simplicity, the approximation  $l \approx L$  is considered here.

Following the reasoning in the paragraphs above, we also assume that: edge lengths  $L$  and initial gap widths  $l$  are  $\sim 10 \mu\text{m}$ ; the lattice constant of the material is  $a \approx 0.3 \text{ nm}$  (which differs  $\lesssim 20\%$  from graphene and several TMDs);  $\epsilon = 0.1$ , meaning kink detachment rate  $10^2$  times smaller than the attachment rate; the condition  $F/Q \leq 10$  is fulfilled.

From equation (4), the maximal roughness of the grain edges in these conditions is  $\sim 40 \text{ nm}$ . However, equation (3) predicts that the minimal roughness attained by the GB is  $\sim 2 \text{ nm}$ , corresponding to a decrease by a factor  $\sim 20$ . The time to attain the minimal roughness can be determined from equation (6) in terms of the attachment rate:  $Qt_{\min} \sim 4 \times 10^6$ .

For comparison, if near-equilibrium growth conditions are chosen and the GB relaxes to its equilibrium configuration, the approach of section S.III of the supplementary material predicts the GB roughness:

$$W_{eq} = \sqrt{\frac{\epsilon a L}{6}} \left( \frac{1}{1-\epsilon} \right). \quad (7)$$

With the above parameters, we obtain  $W_{eq} \sim 7 \text{ nm}$ , which is 3.5 times larger than the expected minimal roughness. The time of crossover to the equilibrium roughness is obtained from the EW kinetics of the GB in section S.III of the supplementary material:

$$Qt_{eq} = \frac{\pi}{144} \left( \frac{L}{a} \right)^2 \frac{1}{\epsilon^2} \left( \frac{1+\epsilon}{1-\epsilon} \right). \quad (8)$$

It gives  $Qt_{eq} \sim 3 \times 10^9$ , which exceeds by three orders of magnitude the time to obtain the minimal roughness in the high coverage regime.

This comparison clearly shows that the advantages of growing 2D materials in the high deposition rate regime can be extrapolated from our nanoscale simulations to typical experimental conditions with microscale grains. The decrease of the GB roughness up to the minimum can be observed in a much shorter time than that necessary for the GB to reach its equilibrium value, which is larger than that minimum.

Our model has the limitation that the mobile particle attachment is restricted to the topmost point of each column  $x$ . This leads to unstable patterns that look very different from those of experiments and of models for specific materials. However, we believe that this limitation does not have significant effect

on our prediction of a minimal roughness for the high deposition rate regime. If that condition for the attachment is relaxed, then the aggregation of mobile particles to the sides of the rough edges may lead to overhang formation. Such overhangs will encapsulate mobile particles, but their positions are effectively frozen and they will eventually attach at those positions to fill the overhangs. It is possible that this process creates lateral correlations along the edges, but such fluctuations, which are correlated at small scales, can be suppressed approximately in the same way as the totally uncorrelated fluctuations considered here.

#### 4. Conclusion

A model for the propagation of two grain edges of a 2D material and for the relaxation of the GB formed after the collision of those edges was proposed. Simple kinetic rules are considered for attachment and detachment of particles from the edges and for particle diffusion while there is a gap between them. This allowed to perform kMC simulations for broad ranges of parameters and investigate their consequences on the geometry of the GBs. The model is expected to be qualitatively applicable for growth with unary precursors, such as methane vapour to produce graphene, but may also be applied to TMDs if the precursor reactions form diffusing growth units uniformly distributed in the gap between the grains (precursor flux obeying the reaction stoichiometry is a plausible condition for that).

The well-known near-equilibrium (attachment-limited) and unstable (diffusion-limited) growth regimes are recovered in the simulations, which shows the reliability of the approach to predict qualitative features of the grain evolution in 2D materials. The simulations also show a distinct third regime when the precursor flux is sufficiently high to fully cover the gap between the edges with growth units (mobile particles) before they begin to attach to those edges. In this high deposition rate regime, an uncorrelated edge roughening is observed until the edges collide. These conditions may produce an initial GB with large roughness, but we show that this boundary relaxes to configurations with a roughness smaller than those of the other regimes in a shorter time. Numerical predictions of the minimal roughness and of the time to attain such configuration are in good agreement with a theoretical approach for the GB relaxation.

To investigate the possible extension of the above results to real grains of 2D materials, the simulation results (obtained at nanoscale) were extrapolated to edges and gaps sizes  $\sim 10 \mu\text{m}$ . It shows that the high coverage regime can produce GBs with minimal roughness  $\sim 2 \text{ nm}$ , which is  $\sim 3.5$  times smaller than the roughness obtained in a near-equilibrium, stationary state. Moreover, the time to obtain that minimal roughness is three orders of magnitude smaller than the expected time for the GB to reach

that stationary state. Thus, if the control of the growth permits to reach a condition in which the gap between neighbouring grains is fully covered by non-aggregated material and if the relaxation dynamics is similar to that proposed here, it is possible that a novel route for efficient growth of that material with very smooth GBs can be developed. Recent advances in microscopy methods allow accurate measurements of nanoscale fluctuations of GBs and may help such studies [55, 56].

#### Data availability statement

The data that support the findings of this study are available upon reasonable request from the authors.

#### Acknowledgments

F D A A R acknowledges support from the Brazilian agencies CNPq (305391/2018-6), FAPERJ (E-26/110.129/2013, E-26/202.881/2018), CAPES (88887.310427/2018-00—PrInt), and from CNRS (France). O P L acknowledges support from CAPES (88887.369967/2019-00).

#### ORCID iDs

Fabio D A Aarão Reis  <https://orcid.org/0000-0002-9054-1083>

Olivier Pierre-Louis  <https://orcid.org/0000-0003-4855-4822>

#### References

- [1] Dong J, Zhang L and Ding F 2019 Kinetics of graphene and 2D materials growth *Adv. Mater.* **31** 1801583
- [2] Huang P Y *et al* 2011 Grains and grain boundaries in single-layer graphene atomic patchwork quilts *Nature* **469** 389–92
- [3] Xu X *et al* 2016 Ultrafast growth of single-crystal graphene assisted by a continuous oxygen supply *Nature Nanotech.* **11** 930–5
- [4] Taslim A B, Nakajima H, Lin Y-C, Uchida Y, Kawahara K, Okazaki T, Suenaga K, Hibino H and Ago H 2019 Synthesis of sub-millimeter single-crystal grains of aligned hexagonal boron nitride on an epitaxial Ni film *Nanoscale* **11** 14668
- [5] Ying H, Moore A, Cui J, Liu Y, Li D, Han S, Yao Y, Wang Z, Wang L and Chen S 2020 Tailoring the thermal transport properties of monolayer hexagonal boron nitride by grain size engineering *2D Mater.* **7** 015031
- [6] Lin J *et al* 2021 Large-area growth of MoS<sub>2</sub> at temperatures compatible with integrating back-end-of-line functionality *2D Mater.* **8** 025008
- [7] Liu L *et al* 2021 Grain-boundary-rich polycrystalline monolayer WS<sub>2</sub> film for attomolar-level Hg<sup>2+</sup> sensors *Nat. Commun.* **12** 3870
- [8] Sangwan V K, Lee H-S, Bergeron H, Balla I, Beck M E, Chen K-S and Hersam M C 2018 Multi-terminal memristors from polycrystalline monolayer molybdenum disulfide *Nature* **554** 500–4
- [9] Zhou Y, Sarwat S G, Jung G S, Buehler M J, Bhaskaran H and Warner J H 2019 Grain boundaries as electrical conduction channels in polycrystalline monolayer WS<sub>2</sub> *ACS Appl. Mater. Interfaces* **11** 10189–97

[10] Zhang Z, Yang Y, Xu F, Wang L and Yakobson B I 2015 Unraveling the sinuous grain boundaries in graphene *Adv. Funct. Mater.* **25** 367–73

[11] Zhang H, Yu Y, Dai X, Yu J, Xu H, Wang S, Ding F and Zhang J 2021 Probing atomic-scale fracture of grain boundaries in low-symmetry 2D materials *Small* **17** 2102739

[12] Ryu J *et al* 2014 Fast synthesis of high-performance graphene films by hydrogen-free rapid thermal chemical vapor deposition *ACS Nano* **8** 950–6

[13] Lee G-H *et al* 2013 High-strength chemical-vapor-deposited graphene and grain boundaries *Science* **340** 1073–6

[14] Artyukhov V I, Liu Y and Yakobson B I 2012 Equilibrium at the edge and atomistic mechanisms of graphene growth *Proc. Natl Acad. Sci.* **109** 15136–40

[15] Bets K V, Artyukhov V I and Yakobson B I 2021 Kinetically determined shapes of grain boundaries in graphene *ACS Nano* **15** 4893–900

[16] Chen S, Gao J, Srinivasan B M, Zhang G, Yang M, Chai J, Wang S, Chi D and Zhang Y-W 2019 Revealing the grain boundary formation mechanism and kinetics during polycrystalline MoS<sub>2</sub> growth *ACS Appl. Mater. Int.* **11** 46090–100

[17] Momeni K *et al* 2020 Multiscale computational understanding and growth of 2D materials: a review *npj Comput. Mater.* **6** 22

[18] Hickey D R *et al* 2021 Illuminating invisible grain boundaries in coalesced single-orientation WS<sub>2</sub> monolayer films *Nano Lett.* **21** 6487–95

[19] Hao Y *et al* 2013 The role of surface oxygen in the growth of large single-crystal graphene on copper *Science* **342** 720–3

[20] Nie S, Wofford J M, Bartelt N C, Dubon O D and McCarty K F 2011 Origin of the mosaicity in graphene grown on Cu(111) *Phys. Rev. B* **84** 155425

[21] Meca E, Lowengrub J, Kim H, Mattevi C and Shenoy V B 2013 Epitaxial graphene growth and shape dynamics on copper: phase-field modeling and experiments *Nano Lett.* **13** 5692–7

[22] Wu P, Zhang Y, Cui P, Li Z, Yang J and Zhang Z 2015 Carbon dimers as the dominant feeding species in epitaxial growth and morphological phase transition of graphene on different Cu substrates *Phys. Rev. Lett.* **114** 216102

[23] Zhuang J, Zhao R, Dong J, Yand T and Ding F 2016 Evolution of domains and grain boundaries in graphene: a kinetic Monte Carlo simulation *Phys. Chem. Chem. Phys.* **18** 2932–9

[24] Yue R *et al* 2017 Nucleation and growth of WSe<sub>2</sub>: enabling large grain transition metal dichalcogenides *2D Mater.* **4** 045019

[25] Srinivasan B M, Hao Y, Hariharaputran R, Rywkin S, Hone J C, Colombo L, Ruoff R S and Zhang Y-W 2018 Oxygen-promoted chemical vapor deposition of graphene on copper: a combined modeling and experimental study *ACS Nano* **12** 9372–80

[26] Michely T and Krug J 2003 *Islands, Mounds and Atoms* (Berlin: Springer)

[27] Pimpinelli A and Villain J 1998 *Physics of Crystal Growth* (Cambridge: Cambridge University Press)

[28] Saito Y 1996 *Statistical Physics of Crystal Growth* (Singapore: World Scientific)

[29] Evans J W, Thiel P A and Bartelt M C 2006 Morphological evolution during epitaxial thin film growth: formation of 2D islands and 3D mounds *Surf. Sci. Rep.* **61** 1–128

[30] Misbah C, Pierre-Louis O and Saito Y 2010 Crystal surfaces in and out of equilibrium: a modern view *Rev. Mod. Phys.* **82** 981–1040

[31] Einax M, Dieterich W and Maass P 2013 Colloquium: Cluster growth on surfaces: densities, size distributions and morphologies *Rev. Mod. Phys.* **85** 921–39

[32] Gaillard P, Chanier T, Henrard L, Moskovkin P and Lucas S 2015 Multiscale simulations of the early stages of the growth of graphene on copper *Surf. Sci.* **637–638** 11–18

[33] Enstone G, Brommer P, Quigley D and Bell G R 2016 Enhancement of island size by dynamic substrate disorder in simulations of graphene growth *Phys. Chem. Chem. Phys.* **18** 15102–9

[34] Barabási A-L and Stanley H E 1995 *Fractal Concepts in Surface Growth* (New York: Cambridge University Press)

[35] Krug J 1997 Origins of scale invariance in growth processes *Adv. Phys.* **46** 139–282

[36] Pismen L M 2006 *Patterns and Interfaces in Dissipative Dynamics* (Springer Series in Synergetics) (Berlin: Springer)

[37] Niu T, Zhou M, Zhang J, Feng Y and Chen W 2013 Growth intermediates for CVD graphene on Cu(111): carbon clusters and defective graphene *J. Am. Chem. Soc.* **135** 8409–14

[38] Loginova E, Bartelt N C, Feibelman P J and McCarty K F 2008 Evidence for graphene growth by C cluster attachment *New. J. Phys.* **10** 093026

[39] Zhang W, Wu P, Li Z and Yang J 2011 First-principles thermodynamics of graphene growth on Cu surfaces *J. Phys. Chem. C* **115** 17782–7

[40] Cui F *et al* 2016 Tellurium-assisted epitaxial growth of large-area, highly crystalline ReS<sub>2</sub> atomic layers on mica substrate *Adv. Mater.* **28** 5019–24

[41] Oliveira T J and Aarão Reis F D A 2013 Scaling in reversible submonolayer deposition *Phys. Rev. B* **87** 235430

[42] Gagliardi L and Pierre-Louis O 2022 Controlling anisotropy in 2D microscopic models of growth *J. Comput. Phys.* **452** 110936

[43] Saito Y, Dufay M and Pierre-Louis O 2012 Nonequilibrium cluster diffusion during growth and evaporation in two dimensions *Phys. Rev. Lett.* **108** 245504

[44] Aarão Reis F D A and Pierre-Louis O 2018 Interface collisions *Phys. Rev. E* **97** 040801(R)

[45] Marguet B, Aarão Reis F D A and Pierre-Louis O 2022 Interface collisions with diffusive mass transport *Phys. Rev. E* **106** 014802

[46] Edwards S F and Wilkinson D R 1982 The surface statistics of a granular aggregate *Proc. R. Soc. A* **381** 17–31

[47] de Assis T A and Reis F D A A 2014 Relaxation after a change in the interface growth dynamics *Phys. Rev. E* **89** 062405

[48] de Assis T A and Reis F D A A 2015 Smoothening in thin-film deposition on rough substrates *Phys. Rev. E* **92** 052405

[49] Pierre-Louis O and Misbah C 1998 Dynamics and fluctuations during MBE on vicinal surfaces. I. Formalism and results of linear theory *Phys. Rev. B* **58** 2259–75

[50] Yao W, Wu B and Liu Y 2020 Growth and grain boundaries in 2D materials *ACS Nano* **14** 9320–46

[51] Cai H, Yu Y, Puretzky A A, Lin Y-C, Geohegan D B and Xiao K 2021 Heterogeneities at multiple length scales in 2D layered materials: from localized defects and dopants to mesoscopic heterostructures *Nano Res.* **14** 1625–49

[52] Dong J, Zhang L, Wu B, Ding F and Liu Y 2021 Theoretical study of chemical vapor deposition synthesis of graphene and beyond: challenges and perspectives *J. Phys. Chem. Lett.* **12** 7942–63

[53] Han Z, Li L, Jiao F, Yu G, Hua W, Wei Z and Geng D 2021 Continuous orientated growth of scaled single-crystal 2D monolayer films *Nanoscale Adv.* **3** 6545–67

[54] Wei Z, Wang Q, Li L, Yang R and Zhang G 2021 Monolayer MoS<sub>2</sub> epitaxy *Nano Res.* **14** 1598–608

[55] Annevelink E, Wang Z-J, Dong G, Johnson H T and Pochet P 2021 A moiré theory for probing grain boundary structure in graphene *Acta Mater.* **217** 117156

[56] Bokai K A *et al* 2021 Visualization of graphene grain boundaries through oxygen intercalation *Appl. Surf. Sci.* **565** 150476